

Composition and hygroscopicity of aerosol particles at Mt. Lu in South China

Li, Weijun; Chi, Jianwei; Shi, Zongbo; Wang, Xinfeng; Chen, Bin; Wang, Yan; Li, Tao; Chen, Jianmin; Zhang, Daizhou; Wang, Zifa; Shi, Chune; Liu, Liangke; Wang, Wenxing

DOI:

[10.1016/j.atmosenv.2014.06.003](https://doi.org/10.1016/j.atmosenv.2014.06.003)

License:

Unspecified

Document Version

Peer reviewed version

Citation for published version (Harvard):

Li, W, Chi, J, Shi, Z, Wang, X, Chen, B, Wang, Y, Li, T, Chen, J, Zhang, D, Wang, Z, Shi, C, Liu, L & Wang, W 2014, 'Composition and hygroscopicity of aerosol particles at Mt. Lu in South China: implications for acid precipitation', *Atmospheric Environment*, vol. 94, pp. 626-636. <https://doi.org/10.1016/j.atmosenv.2014.06.003>

[Link to publication on Research at Birmingham portal](#)

Publisher Rights Statement:

NOTICE: this is the author's version of a work that was accepted for publication in *Atmospheric Environment*. Changes resulting from the publishing process, such as peer review, editing, corrections, structural formatting, and other quality control mechanisms may not be reflected in this document. Changes may have been made to this work since it was submitted for publication. A definitive version was subsequently published in *Atmospheric Environment*, Volume 94, September 2014, Pages 626–636
DOI: 10.1016/j.atmosenv.2014.06.003
Checked for repository 30/10/2014

General rights

Unless a licence is specified above, all rights (including copyright and moral rights) in this document are retained by the authors and/or the copyright holders. The express permission of the copyright holder must be obtained for any use of this material other than for purposes permitted by law.

- Users may freely distribute the URL that is used to identify this publication.
- Users may download and/or print one copy of the publication from the University of Birmingham research portal for the purpose of private study or non-commercial research.
- User may use extracts from the document in line with the concept of 'fair dealing' under the Copyright, Designs and Patents Act 1988 (?)
- Users may not further distribute the material nor use it for the purposes of commercial gain.

Where a licence is displayed above, please note the terms and conditions of the licence govern your use of this document.

When citing, please reference the published version.

Take down policy

While the University of Birmingham exercises care and attention in making items available there are rare occasions when an item has been uploaded in error or has been deemed to be commercially or otherwise sensitive.

If you believe that this is the case for this document, please contact UBIRA@lists.bham.ac.uk providing details and we will remove access to the work immediately and investigate.

Accepted Manuscript

Composition and hygroscopicity of aerosol particles at Mt. Lu in South China:
Implications for acid precipitation

Weijun Li , Jianwei Chi , Zongbo Shi , Xinfeng Wang , Bin Chen , Yan Wang , Tao
Li , Jianmin Chen , Daizhou Zhang , Zifa Wang , Chune Shi , Liangke Liu , Wenxing
Wang

PII: S1352-2310(14)00449-X

DOI: [10.1016/j.atmosenv.2014.06.003](https://doi.org/10.1016/j.atmosenv.2014.06.003)

Reference: AEA 13027

To appear in: *Atmospheric Environment*

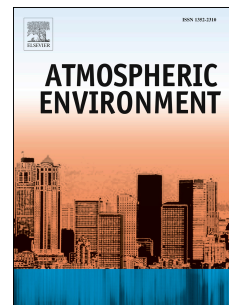
Received Date: 25 February 2014

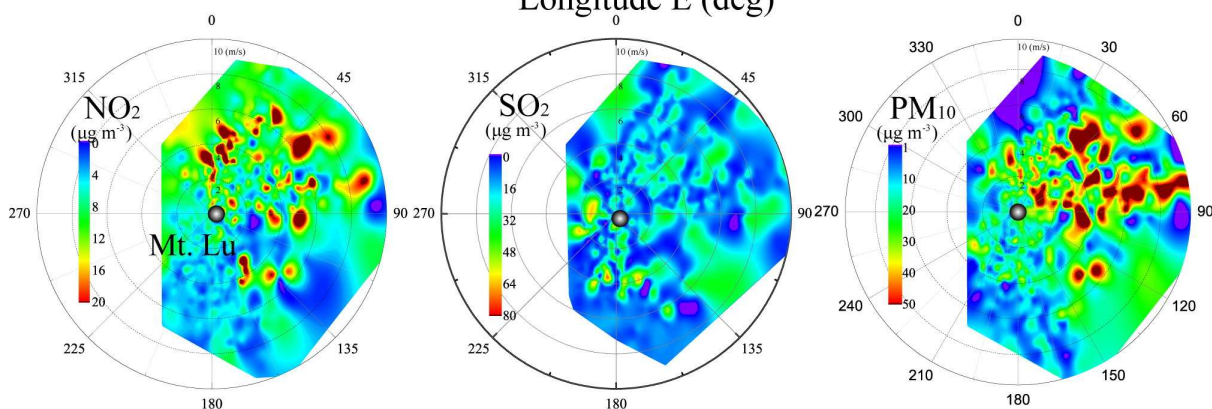
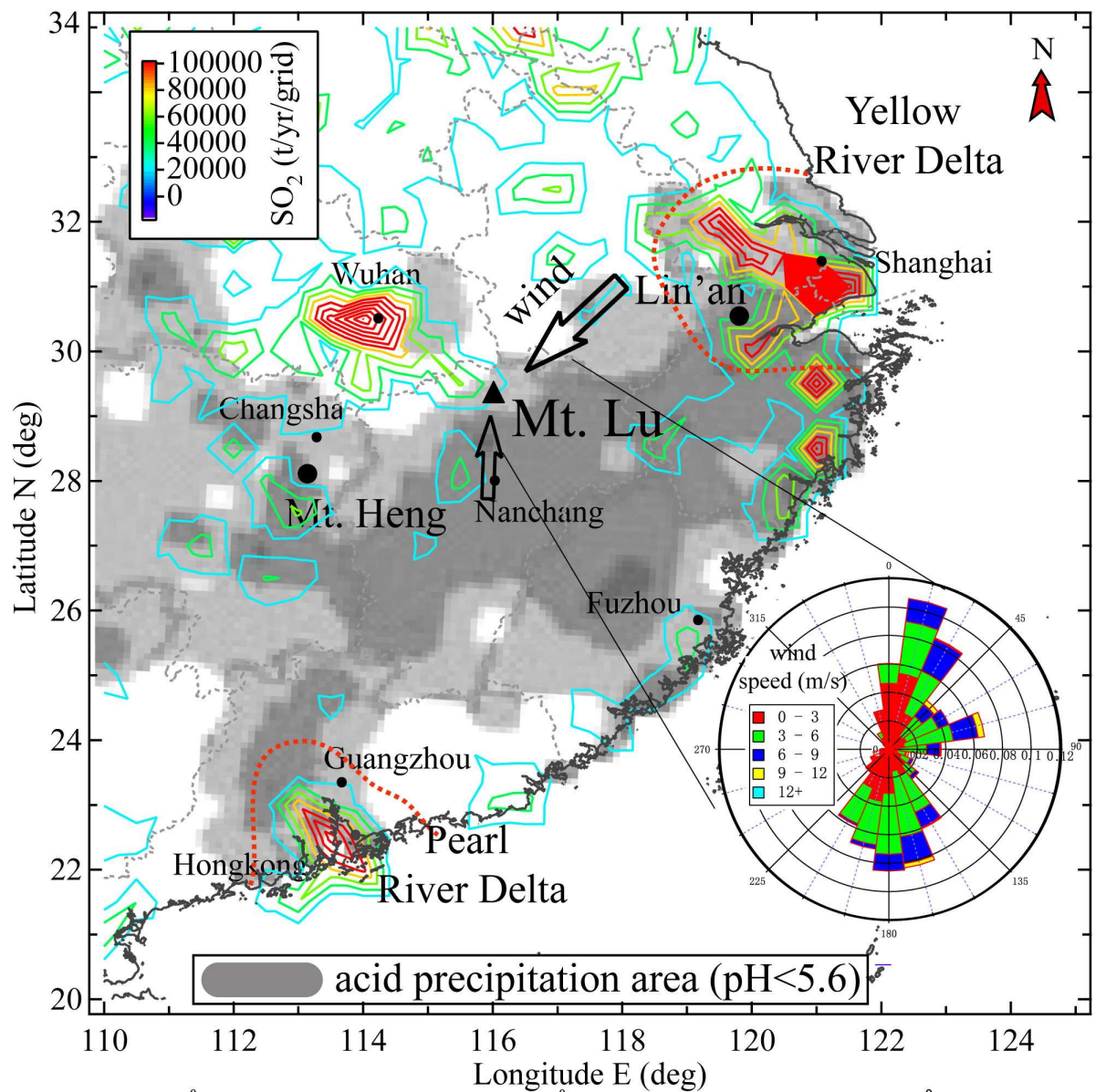
Revised Date: 1 June 2014

Accepted Date: 2 June 2014

Please cite this article as: Li, W., Chi, J., Shi, Z., Wang, X., Chen, B., Wang, Y., Li, T., Chen, J., Zhang, D., Wang, Z., Shi, C., Liu, L., Wang, W., Composition and hygroscopicity of aerosol particles at Mt. Lu in South China: Implications for acid precipitation, *Atmospheric Environment* (2014), doi: 10.1016/j.atmosenv.2014.06.003.

This is a PDF file of an unedited manuscript that has been accepted for publication. As a service to our customers we are providing this early version of the manuscript. The manuscript will undergo copyediting, typesetting, and review of the resulting proof before it is published in its final form. Please note that during the production process errors may be discovered which could affect the content, and all legal disclaimers that apply to the journal pertain.





Composition and hygroscopicity of aerosol particles at Mt. Lu in

South China: Implications for acid precipitation

Weijun Li^{1*}, Jianwei Chi¹, Zongbo Shi², Xinfeng Wang¹, Bin Chen¹, Yan Wang³, Tao Li³, Jianmin Chen^{1,3*}, Daizhou Zhang⁴, Zifa Wang⁵, Chune Shi⁶, Liangke Liu⁷, Wenxing Wang¹

¹Environment Research Institute, Shandong University, Jinan, Shandong 250100, China

²School of Geography, Earth and Environmental Sciences, University of Birmingham, UK

³School of Environment Science and Engineering, Shandong University, Jinan, Shandong 250100, China

⁴Faculty of Environmental and Symbiotic Sciences, Prefectural University of Kumamoto, Kumamoto 862-8502, Japan

⁵State Key of Laboratory of Atmospheric Boundary Physics and Atmospheric Chemistry, Institute of Atmospheric Physics, Chinese Academy of Sciences, Beijing 100029, China

⁶Anhui Institute of Meteorological Sciences, Anhui Institute of Meteorological Sciences, Hefei, 230031 China

⁷Nanjing University of information science and technology, Jiangsu, 210044 China

Corresponding Email: liweijun@sdu.edu.cn (W.J. Li) and jmchen@sdu.edu.cn (J.M. Chen), Environment Research Institute, Shandong University, Jinan, Shandong 250100, China. Tel: +086-531-88364675

Final version submitted to Atmospheric Environment

1 **Abstract:** Physicochemical properties of aerosol particles were studied at Mt. Lu, an
2 elevated site (115°59'E, 29°35'N, 1,165 m) within the acid precipitation area.
3 Northeast winds transport copious amounts of air pollutants and water vapor from the
4 Yangtze River Delta into this acid precipitation area. NH_4^+ and SO_4^{2-} are the dominant
5 ions in $\text{PM}_{2.5}$ and determine aerosol acidity. Individual particle analysis shows
6 abundant S-rich and metals (i.e. Fe-, Zn-, Mn-, and Pb-rich) particles. Unlike aerosol
7 particles in North China and urban areas, there are little soot and mineral particles at
8 Mt. Lu. Lack of mineral particles contributed to the higher acidity in precipitation in
9 the research area. Nano-sized spherical metal particles were observed to be embedded
10 in 37% of S-rich particles. These metal particles were likely originated from heavy
11 industries and fired-power plants. Hygroscopic experiments show that most particles
12 start to deliquesce at 73-76% but organic coating lowers the particle deliquescence
13 relative humidity (DRH) to 63-73%. The DRHs of these aerosol particles are clearly
14 smaller than that of pure ammonium sulfate particles which is 80%. Since RH in
15 ambient air was relatively high, ranging from 65% to 85% during our study period,
16 most particles at our sampling site were in liquid phase. Our results suggest that liquid
17 phase reactions in aerosol particles may contribute to SO_2 to sulfuric acid conversion
18 in the acid precipitation area.

19 **Keywords:** acid precipitation, hygroscopicity, aerosol formation, individual particle

20

21 1. Introduction

22 Airborne pollutants are deposited on the earth's surface by 1) wet deposition (rain
23 and snow); 2) dry deposition (particles and gases). Acting as condensation cloud
24 nuclei (CCN) and ice nuclei (IN), aerosol particles influence the climate system
25 indirectly by altering cloud microphysics and albedo (IPCC, 2007), hydrological
26 balance (Ramanathan et al., 2001), and the ecosystem (Bormann, 1985). In the past
27 two decades, rapid industrialization and urbanization in China have contributed large
28 quantities of anthropogenic pollutants into the atmosphere.

29 Recently, research activities in China has been directed to understand the
30 formation of haze-fog events in East China, with the Chinese government starting to
31 improve air quality in the megacities (Zhang et al., 2012). On the other hand, acid
32 precipitation has been to some extent overlooked, even though it covers 12.9% of the
33 continental area of China (AEAERC, 2011). The world's third largest acid rain area
34 has emerged in this region in the past thirty years, following Europe and North
35 America (Galloway et al., 1987; Wang and Wang, 1995; Li et al., 2010b; Tang et al.,
36 2010). The impact of anthropogenic air pollutants on precipitation composition and
37 the subsequent effects on aquatic and terrestrial ecosystems have been well
38 recognized in North America, Scandinavia, South China, and Europe over the past
39 decade (Bormann, 1985; Galloway et al., 1987). Progress report from the U.S.
40 Environmental Protection Agency (EPA, 2006) showed that the developed countries
41 in past decades that have pursued the tenets of the Clean Air Act have substantially
42 reduced the size of the acid precipitation area. Conversely, in South China the acid
43 precipitation area increased slightly and has been shown to occur throughout this
44 period (Tang et al., 2010).

45 The largest, contiguous acid-impacted region is south of the Yangtze River,
46 according to the AEAERC in 2011. Tang et al. (2010) suggest that the center of the
47 severe acid rain area south of the Yangtze River moved eastwards to include Jiangxi
48 and Zhejiang provinces. In the acidic cloud water or rain water of south China, SO_4^{2-}
49 dominates followed by NH_4^+ , NO_3^- , Ca^{2+} , Cl^- , F^- , K^+ , Na^+ , and Mg^{2+} (Lei et al., 1997;
50 Cao et al., 2009; Huang et al., 2009; Huang et al., 2010; Li et al., 2010b; Sun et al.,

51 2010). Recently, Li et al. (2013b) showed that strongly acidic clouds (pH, ~3.5) cover
52 Jiangxi province and form acid rain in summer. The study further suggested that the
53 acidic cloud droplets enhance the soluble efficiency of nano-sized metals in clouds,
54 which may lead to additional adverse impacts on the ecosystem and human health in
55 South China.

56 Once aerosol particles act as CCN, chemical properties of individual aerosol
57 particles can affect the acidity of the corresponding cloud droplet, thereby pointing
58 out the importance of understanding the physicochemical properties of aerosol
59 particles in the acid precipitation area. In particular, the chemical composition of
60 aerosols among various size ranges is a key factor in determining their hygroscopicity,
61 CCN activity, and optical properties (Hudson, 2007). Individual aerosol particles are a
62 complex mixture of inorganic and organic species, and soluble and insoluble species
63 contributed directly or indirectly by anthropogenic and natural sources (Li and Shao,
64 2009; Posfai and Buseck, 2010). When considering the influence of aerosol particles
65 in one region, one first needs to understand their chemical composition and mixing
66 state (Hudson, 2007; Twohy and Anderson, 2008; Posfai and Buseck, 2010; Adachi et
67 al., 2011; Li et al., 2011a). Individual particle analysis by transmission electron
68 microscopy (TEM) has become a reliable technique to characterize aerosol particles
69 which range in size from nanometer to micrometer, as well as provide information on
70 their sources, morphology, and mixing state (Li and Shao, 2009).

71 Hygroscopic characterization of aerosol particles has important implications for
72 their environmental effects (Martin, 2000; Wise et al., 2009; Freney et al., 2010;
73 Peckhaus et al., 2012). If aerosol particles contain highly hygroscopic species such as
74 sulfates, nitrates, or soluble organic acids, they would take up water when the relative
75 humidity (RH) is high enough and grow into cloud droplets at certain supersaturation
76 conditions (Martin, 2000; Hudson, 2007). Water absorbing hygroscopic components
77 can change both diameter and wavelength dependent refractive indices of individual
78 particles (Lack et al., 2009; Adachi et al., 2011). Therefore, it is necessary to quantify
79 the hygroscopicity of aerosol particles in acid precipitation areas with high RH.

80 The objective of this paper is to characterize the chemical composition and

81 hygroscopicity of individual aerosol particles in an acid deposition area in South
82 China. In this study, aerosol samples were collected near the summit of Mt. Lu
83 ($115^{\circ}59'E$, $29^{\circ}35'N$, 1,165 m) in Jiangxi province, the center of the heavy acid
84 precipitation area in South China. Chemical composition and mixing state of
85 individual particles were investigated using transmission electron microscopy (TEM).
86 We also studied the hygroscopicity of individual particles using a newly developed
87 individual particle hygroscopic (IPH) system.

88 **2. Experiments**

89 **2.1 Sampling site**

90 Mt. Lu, covering an area of 300 km² ($115^{\circ}59'E$, $29^{\circ}35'N$, 1,165 m), is located
91 south of Jiujiang city in northern Jiangxi Province, China, between the Yangtze River
92 and Boyang Lake. Mt. Lu is 700 km northwest of the Pearl River Delta (PRD) and
93 400 km southwest of the Yangtze River Delta (YRD) (Figure 1). Mt. Lu lies within
94 the Asian humid continental and tropical monsoon climate zone, where cloud/fog and
95 rain events are common from spring to autumn. Figure 1 shows that the Mt. Lu area is
96 located within the acid precipitation area of South China. The town of Guling on top
97 of Mt. Lu has a population of about 10,000; most residents work in tourism or related
98 services, so relatively little local pollution is produced. There are some large steel and
99 oil refining industries and coal-fired power plants in the YRD and non-ferrous mines
100 associated with non-ferrous mining, smelting, and refining of pure metals in Jiangxi
101 province. Therefore, the major SO₂ emission sources are located in the YRD but
102 outside of Shanghai city.

103 **2.2 Meteorology**

104 The dominant wind direction below 1500 m during the summer season in South
105 China is from the Northeast, which brings water vapor and pollutants into acid
106 precipitation area (Figure S1-S4 in Supporting Information (SI)). The sampling was
107 conducted during 11 August to 23 September, 2013. The average temperature and
108 relative humidity (RH) were 23 °C and 80% during non-cloud periods, respectively.
109 Thirty 48-h air mass back trajectories ending at Mt.Lu from 14 to 24 November were
110 simulated by HYSPLIT model (<http://ready.arl.noaa.gov/HYSPLIT.php>) (Figure S2).
111 Most of air mass back trajecotries were from South and Northeast areas of Mt. Lu in

112 South China.

113 **2.3 Aerosol sampling and analysis**

114 Aerosol particles were collected on copper TEM grids coated with carbon film
115 (carbon type-B, 300-mesh copper, Tianld Co., China) by a single-stage cascade
116 impactor with a 0.5-mm-diameter jet nozzle and an air flow rate of 0.5 l min^{-1} . For
117 these conditions, the calculated size (d_{50}) is $\sim 0.5 \mu\text{m}$ (Marple et al., 1993). Because
118 the air quality has small changes at Mt. Lu, each sampling time was set up at 4 min in
119 non-cloud periods. Clouds or fog frequently occurred during our sampling period.
120 After sample collection, we immediately used optical microscopy with magnification
121 from $\times 500$ to $\times 1200$ to check whether the carbon film and aerosol distribution on the
122 TEM grids were suitable for analysis. Then, the grid was placed in a sealed, dry
123 plastic tube and stored in a desiccator at $25 \text{ }^\circ\text{C}$ and $20 \pm 3\% \text{ RH}$ to minimize exposure
124 to ambient air and preserve it for analysis. Finally, nine samples collected in clear
125 periods during 14 August - 23 September, 2013 were selected and analyzed by TEM.

126 Aerosol particles on the TEM grids were analyzed with a JEM-2100 TEM
127 operated at 200 kV. Particles examined by TEM were dry at the time of observation in
128 the vacuum of the electron microscope. The effects of water, semi-volatile organics,
129 and NH_4NO_3 could not be considered. Elemental composition was determined
130 semi-quantitatively by an energy-dispersive X-ray spectrometer (EDS) that can detect
131 elements heavier than carbon. EDS spectra were collected for only 15 s to minimize
132 radiation exposure and potential beam damage. Copper could not be analyzed because
133 of interferences from the copper TEM grid. EDS data obtained from INCA software
134 under channel 4-5. In this study, TEM images with magnification between $\times 2000$ and
135 $\times 5000$ were quickly obtained from the center to the periphery of each sample. The
136 procedure ensured that the aerosol distribution and morphology over the entire sample
137 was obtained. To understand the morphology, composition, size, and mixing state of
138 each aerosol particle, TEM images were taken and EDS was used to determine the
139 composition of their component parts such as coatings, inclusions, and aggregates. In
140 order to understand elemental distributions in individual aerosol particles, the
141 elemental mapping experiments were conducted by the JEM-2100F TEM with a

142 scanning TEM (STEM) function. Equivalent circle diameter in two dimensions were
143 determined using the iTEM software (Olympus soft imaging solutions GmbH,
144 Germany) (Li et al., 2013a).

145 A MiniVol sampler (Airmetrics, USA) with a constant pumping rate of 5 l min^{-1}
146 was employed to collect $\text{PM}_{2.5}$ on quartz-fiber filters for the analysis of soluble
147 inorganics. Thirty $\text{PM}_{2.5}$ samples and two blank samples as the reference filters were
148 collected in non-cloud periods from 11 August to 23 September, 2011. The sampling
149 periods ranged from 4 hours to 23.5 hours depending on the cloudy and rainy periods
150 in different days. In addition, we collected the cloud water during cloud or fog periods
151 and cloud water was acidic, with a pH of 3.52 at Mt. Lu. The detailed information
152 about cloud water can be found in Li et al. (2013b). The $\text{PM}_{2.5}$ samples were stored at
153 refrigerator at Mt. Lu and were put in one icebox during the transportation from
154 sampling site to our laboratory, which kept the temperature lower than $0 \text{ }^\circ\text{C}$. Five
155 cations (Na^+ , K^+ , NH_4^+ , Ca^{2+} , and Mg^{2+}) and five anions (F^- , Cl^- , NO_2^- , NO_3^- , and
156 SO_4^{2-}) were quantified by ion chromatography (IC). Because of limitation from the IC
157 detection, we only obtained concentration of nine ions (see section 3.2). The hourly
158 mass concentrations of SO_2 , NO_2 , and PM_{10} were provided by an automatic
159 environmental monitoring station, about 5 m from the sampling site. In this study, we
160 obtained valid concentration data of PM_{10} ($n = 1112$ hours), SO_2 (972 hours), and NO_2
161 (493 hours) (Figure 1). Wind speed, wind direction, relative humidity (RH),
162 barometric pressure, and ambient temperature were obtained from the local
163 meteorological station. In this study, the wind vector maps in different altitudes in
164 South China are shown in supplemental material (Figure S3-S4).

165 **2.4 Hygroscopic experiments of individual aerosol particles**

166 One individual particle hygroscopic (IPH) system was built for observing
167 hygroscopic properties of individual particles at different relative humidities. The
168 measurement system consisted of three steps: (1) Introducing wet and dry N_2 gas with
169 controlled flow into one chamber, controlled by two mass control flow meters. (2)
170 Setting the TEM grids with aerosols on the bottom of one stainless steel column
171 chamber (size: 20mm (height) \times 30mm (diameter)) with two holes on top and bottom

172 side covered by two microscope slides. RH and temperature sensors of a digital
173 hygrometer (Testo 645, $\pm 1\%$) were inserted into the chamber from its side. (3)
174 Obtaining images in different relative humidity through one inverted microscope
175 (IBE2003, China) with a camera (Canon 650D). NaCl aerosols were generated from 1
176 M solutions. We used the same procedure from Wise et al. (2005) to make the
177 standard samples in the laboratory. Laboratory-generated NaCl particles on TEM
178 grids were used to calibrate the system (Figure S5). Detailed descriptions of the
179 similar measurement system were given by Ahn et al. (2010). Similar IPH systems
180 have successfully observed hygroscopic growth observations of field-collected and
181 laboratory-generated aerosols with the diameter larger than $0.5 \mu\text{m}$ (Ahn et al., 2010;
182 Peckhaus et al., 2012; You et al., 2012). Here two samples of particles with organic
183 coating and particles with non-coating were chosen to observe particle hygroscopic
184 growth. The IPH system observed the particle deliquescence and efflorescence at the
185 RH range from 3% to 90% under one stable room temperature at 20°C .

186 **3. Results and discussion**

187 **3.1 Transport of gas and aerosol pollutants**

188 Wind direction and wind speed are the most important factors for transport of air
189 pollutants in the troposphere. Examining wind direction, wind speed, and pollutants at
190 Mt. Lu, Figure 1 shows two major transport paths: from the northeast and from the
191 south. Figure S3 shows that mean wind in August and September is from the northeast.
192 These results were consistent with 48-h air mass back trajectories as shown in Figure
193 S2. The northeasterly wind apparently brought air pollutants and water vapor from the
194 coastal YRD into the acid precipitation area. 42% (by hour) PM_{10} data, 46% SO_2 , and
195 42% NO_2 occur with northeast winds, with their average hourly concentrations at 28
196 $\mu\text{g m}^{-3}$, $16 \mu\text{g m}^{-3}$, and $11 \mu\text{g m}^{-3}$, respectively (Figure 1). Wind rose data (bottom of
197 Figure 1) also showed a possible source of PM_{10} from the northeast direction, that is,
198 the YRD. The southerly wind possibly brought air pollutants from Jiangxi province.
199 37% PM_{10} data, 31% SO_2 , and 37% NO_2 occur from northeast winds, with their
200 average hourly concentrations at $15 \mu\text{g m}^{-3}$, $17 \mu\text{g m}^{-3}$, and $5 \mu\text{g m}^{-3}$, respectively.
201 Figure 1 also shows that the SO_2 emission sources, including heavy industries and

202 coal-fired power plants, lie within the YRD, indicating that air pollutants from the
203 northeast could have contributed to the air pollution on Mt. Lu. The SO₂ wind rose
204 data did not show any particular emission source in the major wind directions. The
205 reason can be attributed to its relatively short lifetime of SO₂ or the region emission
206 sources.

207 **3.2 Soluble inorganic ions in PM_{2.5}**

208 Nine inorganic ions were quantified in 35 PM_{2.5} samples. Figure 2 shows that the
209 highest inorganic ion is SO₄²⁻ with a concentration of 18.4±8.0 μg m⁻³, close to the
210 17.2 μg m⁻³ at the regional background station of Lin'an and more than two times
211 higher than that at Mt. Heng in Hunan province (Xu et al., 2002; Gao et al., 2012).
212 Sun et al. (2010) showed that SO₄²⁻ was the dominant anion, followed by NO₃⁻, both
213 of which control the acidity of cloud water at Mt. Huang in spring.

214 Interestingly, the mass concentration of NO₃⁻ at 0.71 ± 0.99 μg m⁻³ is lower than
215 1.5 μg m⁻³ at Mt. Heng (Gao et al., 2012). The partition of NO₃⁻ between the gas and
216 particulate phases strongly depends on temperature, with lower temperatures favoring
217 the partition of ammonium nitrate in the particulate phase. Indeed, air temperatures
218 ranging from 19 °C to 29 °C at Mt. Lu in this study are much higher than the
219 springtime temperatures at Mt. Heng (9.8 °C to 16.3 °C). Figure 2 shows that NH₄⁺ at
220 6.68±3.3 μg m⁻³ is the major cation to neutralize acidic components. Additionally, K⁺
221 concentration at 0.65±0.22 μg m⁻³ at Mt. Lu is higher than 0.43 μg m⁻³ at Mt. Heng
222 reported by Gao et al.(2012), who suggested that biomass burning contributed
223 potassium salts in the atmosphere over the precipitation area. The average
224 cation/anion (C/A) ratio is 0.94 in PM_{2.5} samples, suggesting that ammonium sulfate
225 could be the dominant component in the PM_{2.5}.

226 Soluble ions of 54 cloud water samples show that SO₄²⁻ dominated 30% of the
227 total ions in cloud water, following by NH₄⁺ (24%) at Mt. Lu during this period (Yang,
228 2013). Therefore, SO₄²⁻ is the dominant acidic ion in both aerosol particles and cloud
229 droplets and contribute to the acidity of cloud water and rain at Mt. Lu in summer.

230 **3.3 Main individual particle types**

231 Based on elemental composition and morphology of individual particles, we

232 identified six different particle types: S-rich, metal (including fly ash), organic matter,
233 soot, K-rich, and mineral. S-rich particles were a dominant aerosol type in all size
234 ranges, which are internally mixed with metal, organic matter, soot, K-rich, and
235 mineral (Figure S6). The result is consistent with the SO_4^{2-} as the dominant ion in
236 $\text{PM}_{2.5}$. In the internally mixed particles, various metal particles were embedded within
237 individual S-rich particles, and secondary organic matter coated onto the surface of
238 S-rich particles, as shown in Figure S6 and Figure 3. These observations are
239 consistent with previous studies (Li et al., 2013b) where large amounts of nano-sized
240 metal particles were measured in the atmosphere at Mt. Lu.

241 3.3.1 Sulfates

242 S-rich particles contained S and O, with certain amounts of K, Na, C, and N
243 (Figure 3a). S-rich particles at Mt. Lu could be mainly composed of $(\text{NH}_4)_2\text{SO}_4$ and
244 minor $(\text{NH}_4)\text{HSO}_4$, organic matter, and K_2SO_4 . Although TEM analysis cannot give
245 nitrate information, NH_4NO_3 cannot be excluded in this study according to the soluble
246 ions in $\text{PM}_{2.5}$ shown in Figure 2. Many studies already show that individual secondary
247 particles commonly contain ammonium sulfate and ammonium nitrate in the
248 atmosphere (Whiteaker et al., 2002; Middlebrook et al., 2011; Hao et al., 2013). As a
249 result, we can speculate that individual secondary particles could mainly contain
250 sulfates with other minor particle species.

251 The second dominant type of S-rich particles contain certain amounts of K
252 (Figure 3b). The fraction of K in S-rich particles is lower than K_2SO_4 in Figure 3c. We
253 suggests that certain amounts of potassium salts coexisted in secondary sulfate
254 particles, which has been commonly observed in cloud droplets at Mt. Lu (Li et al.,
255 2013b). TEM analysis revealed that this kind of S-rich particle significantly
256 contributed soluble K^+ to $\text{PM}_{2.5}$ shown in Figure 2. We also found that the S-rich
257 particles were coated frequently by organic matter. Li et al. (2010a) observed similar
258 particles in Beijing air influenced by agricultural biomass burning. In the present
259 study, only small numbers of K_2SO_4 particles were shown in Figure 3b and abundant
260 S-rich particles with minor K were founds at Mt. Lu. Here we can presume that
261 particles (e.g., KCl and K_2SO_4) from biomass burning can transform into S-rich

262 particles with certain amounts of K through processing in cloud droplets or
263 condensations of SO₂ and H₂SO₄.

264 **3.3.2 Metal particles**

265 Numerous metal particles occurred at Mt. Lu and were internally mixed with
266 S-rich particles (Figure 4). One low-magnification TEM image displays ten S-rich
267 particles, six of which include metal inclusions confirmed by EDS. Many metal
268 particles look like an aggregation of several metal particles. Since small sized metal
269 particles have a higher density, they are darker than other aerosol particle types and
270 are therefore easy to be identified. For example, Figure 5 shows two dark dots in the
271 S-rich particle and their composition reveals two metal particles (Fe-rich and Pb-rich).
272 Li et al. (2013b) found four major metal types at Mt. Lu in cloud droplets: Pb-rich
273 (35%), fly ash including minor metals (27%), Fe-rich (23%), and Zn-rich (15%). We
274 still found that Pb, Fe, and Zn in metal particles were the dominant elements in
275 aerosol particles. These metal particles exhibit a nearly spherical shape (e.g., Figure 5),
276 suggesting that they likely come from industrial processes and coal-fired power
277 generation via high-temperature combustion followed by fast cooling (Giere et al.,
278 2006). There are various large steel and oil refining industries and coal-fired power
279 plants in YRD and many non-ferrous smelting industries are distributed throughout
280 Jiangxi province.

281 Li et al. (2013b) show that acidic cloud droplets can dissolve nano-sized metal
282 particles into sulfates. We carefully examined the composition of individual
283 metal-bearing particles. In this study, we found that 37% of S-rich particles had metal
284 inclusions. For example, Figure 6 shows the Sn-O and Pb-S particles were internally
285 mixed with S-rich particles. Once this kind of aerosol particles act as CCN, SO₂
286 oxidation catalyzed by metal ions could be the dominant in-cloud oxidation pathway
287 (Harris et al., 2013).

288 **3.3.3 Soot and mineral particles**

289 Many studies showed that soot and mineral particles were the major particle types
290 in the atmosphere and were commonly found in aerosol samples collected at mountain
291 site and ground level (Li and Shao, 2009; Posfai and Buseck, 2010; Li et al., 2011b).

292 TEM analysis display a rather low number of soot and mineral particles at Mt. Lu
293 (Figure 7). The typical soot particles in Figure S6g were difficult to be found at Mt.
294 Lu and some tiny soot particles were internally mixed with organic or sulfate (Figure
295 3c). A few elongate regular CaSO_4 were detected in the samples but the $\text{Ca}(\text{NO}_3)_2$
296 coated on mineral particles occurring at Mt. Tai and urban cities in North China (Li
297 and Shao, 2009) had been not found at Mt. Lu. In addition, some mineral particles
298 mixed with metal particles as shown in Figure S6e occurred in fine and coarse
299 particles. Such mixed mineral particles were considered as the emissions of industries
300 and fired-power plant instead of natural soil.

301 **3.3.4 Organic matter**

302 Most organic matter was internally mixed with secondary particles at Mt. Lu.
303 Most organic aerosols can not be clearly identified in secondary particles (Figure 3a)
304 although some can be identified as the organic coatings (Figure 3b-c). Therefore, we
305 classified the internally mixed particles of organic and sulfate in Figure 3b as S-rich
306 particle type. Only small number of particles in the samples at Mt. Lu were dominated
307 by organic matter, as shown in Figure S4a.

308 **3.4 Size and mixing of different particle types**

309 Figure 7 shows the relative abundance of 1634 particles from 80 nm to 4 μm .
310 The S-rich particles account for 82% of all analyzed particles and are the dominant
311 particle type in all size bins. 46% of 1388 analyzed S-rich particles were defined as
312 internally mixed particles that include fly ash, metal, soot, or mineral, except for the
313 organic matter that cannot be clearly identified (Figure 5). Although 18% particles
314 were not classified as S-rich particles, they still contained certain amounts of sulfates.
315 In all, morphology, composition, and mixing state of individual particles at Mt. Lu in
316 South China were more homoneneous than those at Mt. Tai (1535m) in North China
317 (Li et al., 2011b). In addition, only 6% of S-rich particles contained soot inclusions at
318 Mt. Lu are much lower than at Mt. Tai in North China where 72% to 83% of S-rich
319 particles included soot inclusions (Li et al., 2011b). The low percentage of soot and
320 mineral particles at Mt. Lu differs from the aerosol distribution in North China where
321 soot and mineral particles were dominant in sizes smaller than 1 μm and larger than 2

322 μm (Li and Shao, 2009; Li et al., 2011b). In addition, 6% and 3% of 1388 S-rich
323 particles mixed soot and mineral particles.

324 **3.5 Hygroscopic properties of individual particles**

325 Hygroscopic properties of individual particles from two different samples exhibit
326 different hygroscopic growth factors. Figure 8a shows that particles collected on 4
327 September begin to grow at 73-76% with the average growth factor (GF) at 1.006 and
328 that dramatic growth occurs at 80% with the average GR at 1.13. Figure 8b shows that
329 particles collected on 5 September begin to grow at 63-73% with the average GR at
330 1.04 but that part of them display dramatic growth at 80% with the average GR at
331 1.23. The dramatic changes of growth factor at 80% suggest that these secondary
332 particles completely transformed from solid phase to liquid phase in two samples.
333 When the humidity increase 90%, the GR values increase the largest at 1.26 in Figure
334 8a and 1.38 in Figure 8b. Additionally, the particles in these two samples have similar
335 dehydration curves with the efflorescence RH (ERH) at 49-53%. Although the
336 particles in the two samples have similar DRH and ERH, they exhibit different
337 hygroscopic growth trends.

338 A number of studies have shown that hygroscopic properties of aerosol particles
339 are dependent on their chemical composition (Martin, 2000; Choi and Chan, 2002;
340 Shi et al., 2012). Figure 2 shows that SO_4^{2-} is the dominant ion in fine particles,
341 consistent with the dominant S-rich particles found in individual particle analysis.
342 Individual ambient particles normally start to deliquesce at lower RH than the DRH at
343 80% of the pure $(\text{NH}_4)_2\text{SO}_4$. This result can be attributable to the mixtures of two or
344 more inorganic species (e.g., $(\text{NH}_4)_2\text{SO}_4$, $(\text{NH}_4)\text{HSO}_4$, K_2SO_4 , or NH_4NO_3) within the
345 same individual particles (discussed in section 3.3.1) (Freney et al., 2009). In
346 particular, particles shown in Figure 8b start to deliquesce at 63-73% -- much lower
347 than those at 73-76% shown in Figure 8a. The ion analysis and TEM observations
348 together showed similar inorganic ions and particle types, but TEM images revealed
349 thin organic layers coated on some particles in Figure 8b. Soluble organic species in
350 the internally mixed particles may cause the water absorption of organic materials at
351 low RH than inorganic materials (Varutbangkul et al., 2006) and change the

352 hygroscopic growth of aerosol particles (Brooks et al., 2002; Choi and Chan, 2002).
353 Therefore, the soluble organic coatings probably induce the early deliquescence of
354 individual particles. Shi et al. (2012) showed that the internally mixed
355 $(\text{NH}_4)_2\text{SO}_4$ -benzoic acid particles display deliquescence earlier than the DRH of pure
356 $(\text{NH}_4)_2\text{SO}_4$ particles. Also, the ratio of organic and inorganic ions in individual
357 particles determines their deliquescent transitions (Peckhaus et al., 2012). These
358 results suggest that soluble organic coatings and mixtures of multi-inorganic species
359 account for the lower DRH of individual particles at Mt. Lu compared to that of
360 ammonium sulfate.

361 The ambient RH during the sampling periods ranged from 65% to 85%. Based on
362 the hygroscopic experiments, we conclude that the some or all the aerosol particles in
363 non-cloud periods suspended as the liquid phase or liquid-solid phase while
364 suspended in air. Therefore, the liquid water around the deliquesced particles provide
365 an important media for gaseous SO_2 to sulfate conversion.

366 **3.6 Implications of acid precipitation**

367 Heavy acid precipitation in South China mostly occurs in highland areas with
368 altitudes of 500-1500 m, where SO_2 emissions are low (Figure S3). Figure 1 shows
369 the largest and highest intense SO_2 emissions in South China in the YRD, one area
370 that is upwind of Mt. Lu in summer. The dominant wind is from the east during
371 sampling periods; therefore, the SO_2 emissions could be readily transported into the
372 acid precipitation area and be transformed into secondary sulfates. Large amounts of
373 secondary particles dominated by SO_4^{2-} can be formed during long-range transport
374 and can further be CCN in acid clouds. Based on the composition and hygroscopicity
375 of aerosols in the present study and results from Harris et al. (2013), we summarized
376 the SO_2 oxidation during long-range transport in Figure S7a. Liquid layer formation
377 on secondary particles due to early deliquescence probably enhance SO_2 oxidation
378 through heterogeneous reactions in multiphase environment (Ravishankara, 1997).

379 Compared to small amounts of mineral and soot particles from ground-level
380 sources such as road dust, ground soil, and vehicle emissions, the abundant metal
381 particles at Mt. Lu suggest that the large amounts of gaseous and particulate emissions

382 from major industries and power plants can reach high altitudes. As a result, transition
383 metals from anthropogenic sources could catalyze SO₂ oxidation in clouds (Harris et
384 al. (2013). In addition, the low concentrations of Ca²⁺ and Mg²⁺ in PM_{2.5} and rather
385 low number of mineral particles from TEM analysis both suggest that the alkaline
386 mineral particles have limited acidic buffering capacity at Mt. Lu. Therefore, absence
387 of mineral particles in the air likely contributes to the higher acidity of aerosol
388 particles. These phenomenon indicated above can be attributed to the seasonal
389 meteorological situation in South China and the height of emission sources -- both
390 critical for determining the transport distance (Kahn et al., 2008; Chen et al., 2013).
391 Firstly, the humid air and frequent rains limit vertical transport of ground-level urban
392 pollutants such as soil dust and vehicle emissions raise up to planetary boundary layer.
393 Secondly, the large industries and power plants with their tall stacks can emit air
394 pollutants into higher atmospheric levels (Chen et al., 2013). Figure S4 shows that
395 wind speed is at 3-10 m/s at 1000 m and < 3 m/s on the ground during the sampling
396 period. Therefore, the pollutants at high altitude can be dispersed quickly and
397 transported for long distance. In addition, biomass burning plumes can reach the free
398 troposphere because their buoyancy can be sufficient to lift smoke above the
399 near-surface boundary layer (Kahn et al., 2008).

400 Based on our results and discussion, we devised one conceptual model that
401 describes air pollutant emissions and their transport in Figure S7b. Massive amounts
402 of air pollutants (e.g., SO₂ and metal) from coal-fired plants, heavy industries, and
403 biomass burning are readily transported into upper levels of the troposphere. The
404 summer monsoons likely drive large amounts SO₂ and water vapor from east lowland
405 areas to west highland areas in South China. Therefore, beside pollutants' emission
406 and transport, regional meteorological properties (i.e. wind and humidity) and terrain
407 also significantly affect acidic cloud formation.

408 **4. Conclusions**

409 Soluble inorganic ions and individual aerosol particles were studied in summer at
410 Mt. Lu. Northeast winds transported air pollutants from the YRD into the acid
411 precipitation area, with the average hourly concentrations at 28 µg m⁻³ for PM₁₀, 16

412 $\mu\text{g m}^{-3}$ SO_2 , and $11 \mu\text{g m}^{-3}$ for NO_2 . SO_4^{2-} is the dominant acidic ion in aerosol
413 particles and could determine the acidity of cloud water and rain at Mt. Lu. In
414 addition, absence of mineral particles in the air lead to their limited acidic buffering
415 capacity and conversely aerosol particles become more acidic at Mt. Lu.

416 The secondary particles occurred in all sizes and S-rich particles were the
417 dominant particle type, accounting for 82% of all analyzed particles. The study
418 indicates that individual particles contain multi-inorganic species with the major
419 compound being $(\text{NH}_4)_2\text{SO}_4$ with lesser amounts of NH_4HSO_4 , NH_4NO_3 , or K_2SO_4 .
420 The hygroscopic experiments show that individual particles start to deliquesce at
421 73-76%, although the secondary particles completely deliquesce at 80%. In addition,
422 the soluble organic coatings on secondary particles can start deliquescence at 63-73%
423 of individual particles but still completely deliquesce at 80%. Considering the ambient
424 RH of 65-85%, the secondary particles should be in the liquid phase or liquid-solid
425 multiphase in air. We found large amounts of nano-sized metal particles embedded in
426 37% S-rich particles. In addition, we devised a conceptual model that describes air
427 pollutant emissions and their transport, clearly indicating the acid cloud or rain
428 formation at Mt. Lu.

429 **Auxiliary Materials Available**

430 **Figure S1** Terrain of South China and terrain profile of from PRD (East) to Mt. Lu
431 (West); **Figure S2** 48-h Back trajectories of air masses arriving at 1500 m at Mt. Lu
432 during 14 August -24 September, 2013; **Figure S3** Topography and Asian summer
433 monsoon.; **Figure S4** Wind direction and speed in different heights in August and
434 September of 2011 in South China; **Figure S5** Humidifying and dehydration curves
435 for the laboratory-generated NaCl particle collected on a TEM grid; **Figure S6**
436 Different types of individual particles based on morphology and compositions; **Figure**
437 **S7** Conceptual model summarizing acid rain or cloud formation from anthropogenic
438 pollutants; **Figure S8** Sulfate particles without/with organic coating from the two
439 different aerosol samples examined by TEM/EDS.

440 **Acknowledgments**

441 We are grateful for the help from Xiaolin Ma and Xiaoheng Zhang from Mountain Lu

442 meteorological station. We appreciate Peter Hyde's comments and proofreading. This
443 work was funded by National Natural Science Foundation of China (41105088,
444 41375126), National Basic Research Program of China (2011CB403401),
445 International Cooperation and Exchanges NSFC-JSPS (41311140168), Fundamental
446 Research Funds of Shandong University (2014QY001-02), and State Key Laboratory
447 of Atmospheric Boundary Physics and Atmospheric Chemistry (LAPC-KF-2013-15).

448 References:

- 449 Adachi, K., Freney, E.J., Buseck, P.R., 2011. Shapes of internally mixed hygroscopic aerosol particles
450 after deliquescence, and their effect on light scattering. *Geophysical Research Letters* 38 (13),
451 L13804, doi:10.1029/2011GL047540.
- 452 AEAERC (2011), Annual Environment Report of China (AEAERC), <http://www.zhb.gov.cn/>.
- 453 Ahn, K.-H., Kim, S.-M., Jung, H.-J., Lee, M.-J., Eom, H.-J., Maskey, S., Ro, C.-U., 2010. Combined
454 Use of Optical and Electron Microscopic Techniques for the Measurement of Hygroscopic
455 Property, Chemical Composition, and Morphology of Individual Aerosol Particles. *Analytical*
456 *Chemistry* 82 (19), 7999-8009.
- 457 Bormann, F.H., 1985. Air Pollution and Forests: An Ecosystem Perspective. *BioScience* 35 (7),
458 434-441.
- 459 Brooks, S.D., Wise, M.E., Cushing, M., Tolbert, M.A., 2002. Deliquescence behavior of
460 organic/ammonium sulfate aerosol. *Geophysical Research Letters* 29 (19),
461 doi:10.1029/2002GL014733.
- 462 Cao, Y.-Z., Wang, S., Zhang, G., Luo, J., Lu, S., 2009. Chemical characteristics of wet precipitation at
463 an urban site of Guangzhou, South China. *Atmospheric Research* 94 (3), 462-469.
- 464 Chen, B., Stein, A.F., Maldonado, P.G., Sanchez de la Campa, A.M., Gonzalez-Castanedo, Y., Castell,
465 N., de la Rosa, J.D., 2013. Size distribution and concentrations of heavy metals in atmospheric
466 aerosols originating from industrial emissions as predicted by the HYSPLIT model. *Atmospheric*
467 *Environment* 71 (0), 234-244.
- 468 Choi, M.Y., Chan, C.K., 2002. The effects of organic species on the hygroscopic behaviors of inorganic
469 aerosols. *Environmental Science & Technology* 36 (11), 2422-2428.
- 470 EPA (2006), Progress report from the U.S. Environmental Protection Agency,

- 471 <http://www.epa.gov/airmarkets/progress/progress-reports.html>.
- 472 Freney, E.J., Martin, S.T., Buseck, P.R., 2009. Deliquescence and Efflorescence of Potassium Salts
473 Relevant to Biomass-Burning Aerosol Particles. *Aerosol Science and Technology* 43 (8), 799 -
474 807.
- 475 Freney, E.J., Adachi, K., Buseck, P.R., 2010. Internally mixed atmospheric aerosol particles:
476 Hygroscopic growth and light scattering. *Journal of Geophysical Research: Atmospheres* 115
477 (D19210), doi:10.1029/2009JD013558.
- 478 Galloway, J., Dianwu, Z., Jiling, X., Likens, G.E., 1987. Acid Rain: China, United States, and a Remote
479 Area. *Science* 236 (4808), 1559-1562.
- 480 Gao, X., Xue, L., Wang, X., Wang, T., Yuan, C., Gao, R., Zhou, Y., Nie, W., Zhang, Q., Wang, W., 2012.
481 Aerosol ionic components at Mt. Heng in central southern China: Abundances, size distribution,
482 and impacts of long-range transport. *Science of The Total Environment* 433 (0), 498-506.
- 483 Giere, R., Blackford, M., Smith, K., 2006. TEM study of PM_{2.5} emitted from coal and tire combustion
484 in a thermal power station. *Environmental Science & Technology* 40 (20), 6235-6240.
- 485 Hao, L., Romakkaniemi, S., Kortelainen, A., Jaatinen, A., Portin, H., Miettinen, P., Komppula, M.,
486 Leskinen, A., Virtanen, A., Smith, J.N., Sueper, D., Worsnop, D.R., Lehtinen, K.E.J., Laaksonen,
487 A., 2013. Aerosol Chemical Composition in Cloud Events by High Resolution Time-of-Flight
488 Aerosol Mass Spectrometry. *Environmental Science & Technology* 47 (6), 2645-2653.
- 489 Harris, E., Sinha, B., van Pinxteren, D., Tilgner, A., Fomba, K.W., Schneider, J., Roth, A., Gnauk, T.,
490 Fahlbusch, B., Mertes, S., Lee, T., Collett, J., Foley, S., Borrmann, S., Hoppe, P., Herrmann, H.,
491 2013. Enhanced Role of Transition Metal Ion Catalysis During In-Cloud Oxidation of SO₂.
492 *Science* 340 (6133), 727-730.
- 493 Huang, D.-Y., Xu, Y.-G., Peng, P.a., Zhang, H.-H., Lan, J.-B., 2009. Chemical composition and
494 seasonal variation of acid deposition in Guangzhou, South China: Comparison with precipitation
495 in other major Chinese cities. *Environmental Pollution* 157 (1), 35-41.
- 496 Huang, X.-F., Li, X., He, L.-Y., Feng, N., Hu, M., Niu, Y.-W., Zeng, L.-W., 2010. 5-Year study of
497 rainwater chemistry in a coastal mega-city in South China. *Atmospheric Research* 97 (1-2),
498 185-193.
- 499 Hudson, J.G., 2007. Variability of the relationship between particle size and cloud-nucleating ability.
500 *Geophysical Research Letters* 34 (L08), doi:10.1029/2006GL028850.

- 501 IPCC (2007), Intergovernmental Panel on Climate Change(2007), Climate Change 2007, in *Climate*
502 *Change 2007: The Physical Science Basis. Contribution of Working Group I to the Fourth*
503 *Assessment Report of the Intergovernmental Panel on Climate Change*, edited by S. Solomon, D.
504 Qin, M. Manning, Z. Chen, M. Marquis, K.B. Averyt, M. TignorH.L. Miller, p. 1056, Cambridge,
505 United Kingdom and New York, 5 NY, USA, 5(topic 2), New York.
- 506 Kahn, R.A., Chen, Y., Nelson, D.L., Leung, F.-Y., Li, Q., Diner, D.J., Logan, J.A., 2008. Wildfire
507 smoke injection heights: Two perspectives from space. *Geophysical Research Letters* 35 (4),
508 L04809.
- 509 Lack, D.A., Quinn, P.K., Massoli, P., Bates, T.S., Coffman, D., Covert, D.S., Sierau, B., Tucker, S.,
510 Baynard, T., Lovejoy, E., Murphy, D.M., Ravishankara, A.R., 2009. Relative humidity
511 dependence of light absorption by mineral dust after long-range atmospheric transport from the
512 Sahara. *Geophysical Research Letters* 36 (24), L24805.
- 513 Lei, H.-C., Tanner, P.A., Huang, M.-Y., Shen, Z.-L., Wu, Y.-X., 1997. The acidification process under
514 the cloud in southwest China: Observation results and simulation. *Atmospheric Environment* 31
515 (6), 851-861.
- 516 Li, W., Li, P., Sun, G., Zhou, S., Yuan, Q., Wang, W., 2011a. Cloud residues and interstitial aerosols
517 from non-precipitating clouds over an industrial and urban area in northern China. *Atmospheric*
518 *Environment* 45 (15), 2488-2495.
- 519 Li, W., Wang, T., Zhou, S., Lee, S., Huang, Y., Gao, Y., Wang, W., 2013a. Microscopic Observation of
520 Metal-Containing Particles from Chinese Continental Outflow Observed from a Non-Industrial
521 Site. *Environmental Science & Technology* 47 (16), 9124-9131.
- 522 Li, W.J., Shao, L.Y., 2009. Transmission electron microscopy study of aerosol particles from the brown
523 hazes in northern China. *Journal of Geophysical Research: Atmospheres* 114 (D09),
524 doi:10.1029/2008JD011285.
- 525 Li, W.J., Shao, L.Y., Buseck, P.R., 2010a. Haze types in Beijing and the influence of agricultural
526 biomass burning. *Atmospheric Chemistry and Physics* 10 (17), 8119-8130.
- 527 Li, W.J., Zhang, D.Z., Shao, L.Y., Zhou, S.Z., Wang, W.X., 2011b. Individual particle analysis of
528 aerosols collected under haze and non-haze conditions at a high-elevation mountain site in the
529 North China plain. *Atmospheric Chemistry and Physics* 11 (22), 11733-11744.
- 530 Li, W.J., Wang, Y., Collett, J.L., Chen, J., Zhang, X., Wang, Z., Wang, W., 2013b. Microscopic

- 531 Evaluation of Trace Metals in Cloud Droplets in an Acid Precipitation Region. *Environmental*
532 *Science & Technology* 47 (9), 4172-4180.
- 533 Li, Y., Yu, X., Cheng, H., Lin, W., Tang, J., Wang, S., 2010b. Chemical characteristics of precipitation
534 at three Chinese regional background stations from 2006 to 2007. *Atmospheric Research* 96 (1),
535 173-183.
- 536 Martin, S.T., 2000. Phase transitions of aqueous atmospheric particles. *Chem. Rev.* 100 (9), 3403-3453.
- 537 Middlebrook, A.M., Bahreini, R., Jimenez, J.L., Canagaratna, M.R., 2011. Evaluation of
538 Composition-Dependent Collection Efficiencies for the Aerodyne Aerosol Mass Spectrometer
539 using Field Data. *Aerosol Science and Technology* 46 (3), 258-271.
- 540 Peckhaus, A., Grass, S., Treuel, L., Zellner, R., 2012. Deliquescence and Efflorescence Behavior of
541 Ternary Inorganic/Organic/Water Aerosol Particles. *The Journal of Physical Chemistry A* 116 (24),
542 6199-6210.
- 543 Posfai, M., Buseck, P.R., 2010. Nature and Climate Effects of Individual Tropospheric Aerosol
544 Particles. *Annual Review of Earth and Planetary Sciences* 38 (1), 17-43.
- 545 Ramanathan, V., Crutzen, P.J., Kiehl, J.T., Rosenfeld, D., 2001. Atmosphere - Aerosols, climate, and the
546 hydrological cycle. *Science* 294 (5549), 2119-2124.
- 547 Ravishankara, A.R., 1997. Heterogeneous and Multiphase Chemistry in the Troposphere. *Science* 276
548 (5315), 1058-1065.
- 549 Shi, Y., Ge, M., Wang, W., 2012. Hygroscopicity of internally mixed aerosol particles containing
550 benzoic acid and inorganic salts. *Atmospheric Environment* 60, 9-17.
- 551 Sun, M., Wang, Y., Wang, T., Fan, S., Wang, W., Li, P., Guo, J., Li, Y., 2010. Cloud and the
552 corresponding precipitation chemistry in south China: Water-soluble components and pollution
553 transport. *Journal of Geophysical Research: Atmospheres* 115 (D22), D22303.
- 554 Tang, J., Xu, X., Ba, J., Wang, S., 2010. Trends of the precipitation acidity over China during
555 1992–2006. *Chin. Sci. Bull.* 55 (17), 1800-1807.
- 556 Twohy, C.H., Anderson, J.R., 2008. Droplet nuclei in non-precipitating clouds: composition and size
557 matter. *Environmental Research Letters* 3 (4), 045002.
- 558 Varutbangkul, V., Brechtel, F.J., Bahreini, R., Ng, N.L., Keywood, M.D., Kroll, J.H., Flagan, R.C.,
559 Seinfeld, J.H., Lee, A., Goldstein, A.H., 2006. Hygroscopicity of secondary organic aerosols
560 formed by oxidation of cycloalkenes, monoterpenes, sesquiterpenes, and related compounds.

- 561 Atmospheric Chemistry and Physics 6 (9), 2367-2388.
- 562 Wang, W., Wang, T., 1995. On the origin and the trend of acid precipitation in China. *Water, Air, & Soil*
563 *Pollution* 85 (4), 2295-2300.
- 564 Whiteaker, J.R., Suess, D.T., Prather, K.A., 2002. Effects of meteorological conditions on aerosol
565 composition and mixing state in Bakersfield, CA. *Environmental Science & Technology* 36 (11),
566 2345-2353.
- 567 Wise, M.E., Biskos, G., Martin, S.T., Russell, L.M., Buseck, P.R., 2005. Phase transitions of single salt
568 particles studied using a transmission electron microscope with an environmental cell. *Aerosol Sci.*
569 *Technol.* 39 (9), 849-856.
- 570 Wise, M.E., Freney, E.J., Tyree, C.A., Allen, J.O., Martin, S.T., Russell, L.M., Buseck, P.R., 2009.
571 Hygroscopic behavior and liquid-layer composition of aerosol particles generated from natural
572 and artificial seawater. *Journal of Geophysical Research-Atmospheres* 114, 8.
- 573 Xu, J., Bergin, M.H., Yu, X., Liu, G., Zhao, J., Carrico, C.M., Baumann, K., 2002. Measurement of
574 aerosol chemical, physical and radiative properties in the Yangtze delta region of China.
575 *Atmospheric Environment* 36 (2), 161-173.
- 576 Yang, X. (2013), Analysis of ionic composition and sources in cloud water at Mount Lu, master thesis,
577 1-83 pp, Shandong University, Jinan (in Chinese).
- 578 You, Y., Renbaum-Wolff, L., Carreras-Sospedra, M., Hanna, S.J., Hiranuma, N., Kamal, S., Smith,
579 M.L., Zhang, X., Weber, R.J., Shilling, J.E., Dabdub, D., Martin, S.T., Bertram, A.K., 2012.
580 Images reveal that atmospheric particles can undergo liquid-liquid phase separations. *Proceedings*
581 *of the National Academy of Sciences of the United States of America* 109 (33), 13188-13193.
- 582 Zhang, Q., Streets, D.G., Carmichael, G.R., He, K.B., Huo, H., Kannari, A., Klimont, Z., Park, I.S.,
583 Reddy, S., Fu, J.S., Chen, D., Duan, L., Lei, Y., Wang, L.T., Yao, Z.L., 2009. Asian emissions in
584 2006 for the NASA INTEX-B mission. *Atmospheric Chemistry and Physics* 9 (14), 5131-5153.
- 585 Zhang, Q., He, K., Huo, H., 2012. Policy: Cleaning China's air. *Nature* 484 (7393), 161-162.
- 586
- 587

588 **Figure Captions**

589 **Figure 1** The location of Mt. Lu ($115^{\circ} 59' E$, $29^{\circ} 35' N$, 1,165 m) in the acid precipitation
590 area wind rose, and concentration distribution for PM_{10} , SO_2 , and NO_2 associated with wind speed
591 and directions from 1 August to 26 September, 2011. Mt. Heng ($27.3^{\circ} N$, $112.7^{\circ} E$, elevation at
592 1269 m) as one elevated site and Lin'an station ($30.3^{\circ} N$, $119.7^{\circ} E$) as one regional background
593 site, are marked in the acid precipitation area. The data of acid precipitation area were obtained
594 from the Annual Environment Report of China in 2011 and the contours represent the SO_2
595 emission distributions in East China (units: t/year/grid, grid size: 0.5 degree, data from Zhang et
596 al.(2009)).

597 **Figure 2** Average soluble inorganic ions concentration in 33 $PM_{2.5}$ samples at Mt. Lu in summer.

598 **Figure 3** Three different types of individual S-rich particles. (a) S-rich particle with minor K
599 mixed with one As-rich particle and one Fe-rich particle. EDS data obtained from INCA software
600 under channel 5. (b) S-rich particle with moderate K coated by organics. (c) K_2SO_4 particle mixed
601 with organic coating, soot, and Pb-S. EDS data obtained from INCA software under channel 4.

602 **Figure 4** One low-magnification TEM image showing metal inclusions in S-rich

603 Figure 5 TEM image and EDS of two metal inclusions in one S-rich particle.

604 **Figure 6** Elemental mapping of an individual metal-bearing particle obtained from the STEM. A
605 dark-field TEM image of the individual particle and each elemental distribution are shown.

606 **Figure 7** Proportions of aerosol particles collected at Mt. Lu during 11 August to 23 September,
607 2011 in acid precipitation area. A total of 1634 aerosol particles were identified by their different
608 morphology and composition. The number of the analyzed aerosol particles in different size
609 ranges is shown above each column.

610 **Figure 8** Deliquescence and efflorescence of each particle with one color from 3% to 90% RH. (a)
611 the sample collected on 4 September, 2011 containing secondary particles (b) the sample collected
612 on 5 September, 2011 containing secondary particles with organic coating. Compositions of
613 individual particles in the two samples were examined by TEM/EDS as shown in Figure S6.
614 Mixing state and composition of individual particles were described in the scheme.

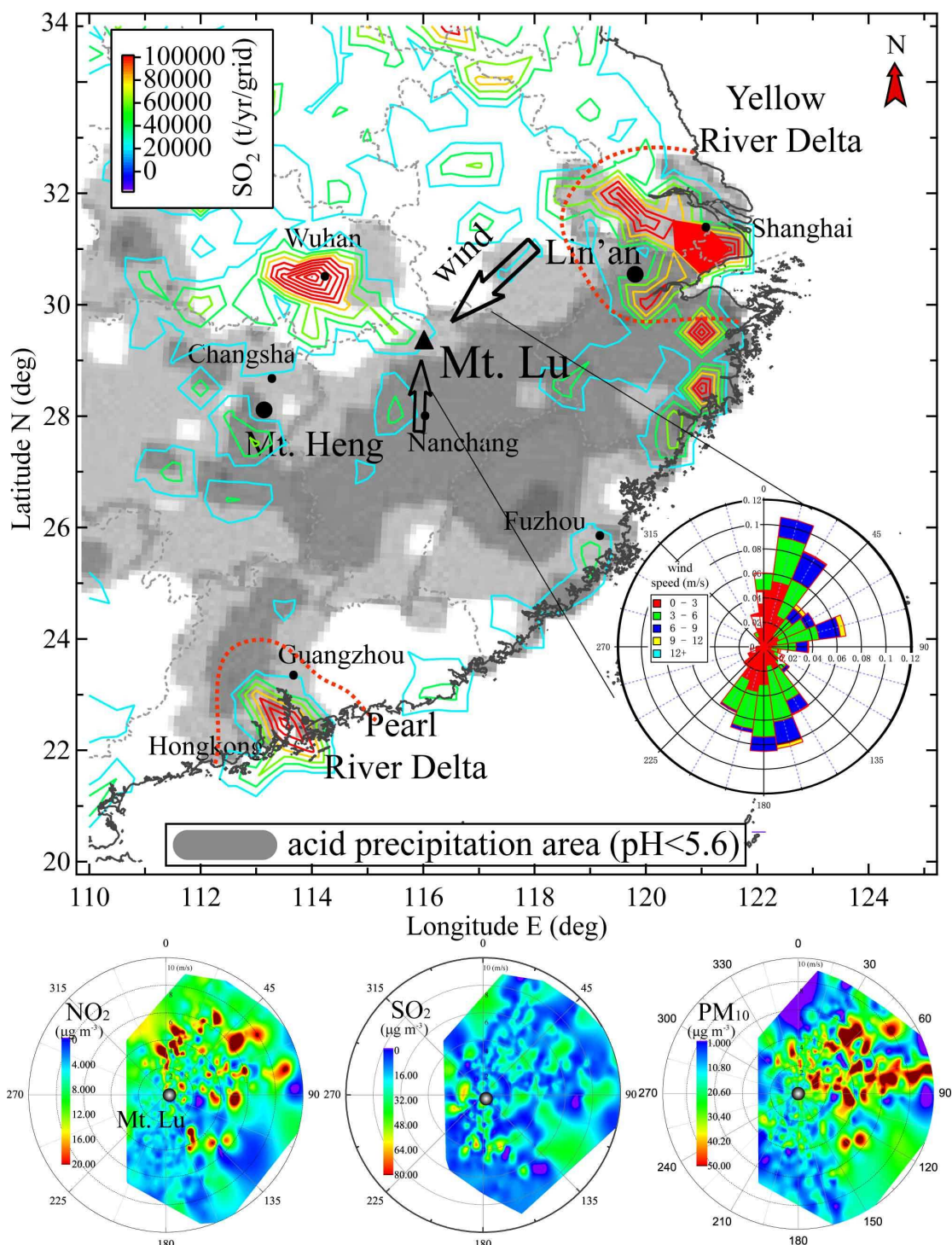


Figure 1 The location of Mt. Lu ($115^{\circ} 59' E$, $29^{\circ} 35' N$, 1,165 m) in the acid precipitation area wind rose, and concentration distribution for PM_{10} , SO_2 , and NO_2 associated with wind speed and directions from 1 August to 26 September, 2011. Mt. Heng ($27.3^{\circ} N$, $112.7^{\circ} E$, elevation at 1269 m) as one elevated site and Lin'an station ($30.3^{\circ} N$, $119.7^{\circ} E$) as one regional background site, are marked in the acid precipitation area. The data of acid precipitation area were obtained from the Annual Environment Report of China in 2011 and the contours represent the SO_2 emission distributions in East China (units: t/year/grid, grid size: 0.5 degree, data from Zhang et al.(2009)).

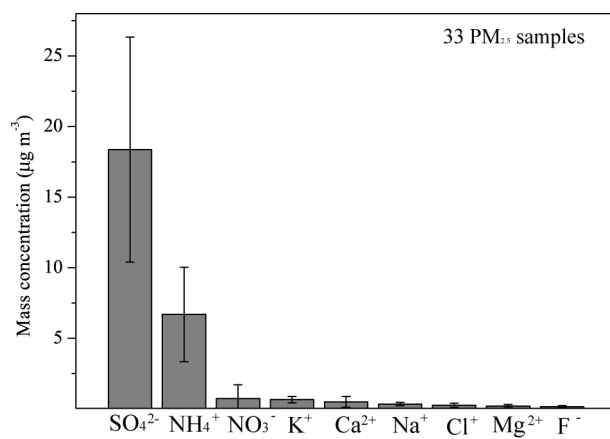


Figure 2 Average soluble inorganic ions concentration in 33 PM_{2.5} samples at Mt. Lu in summer.

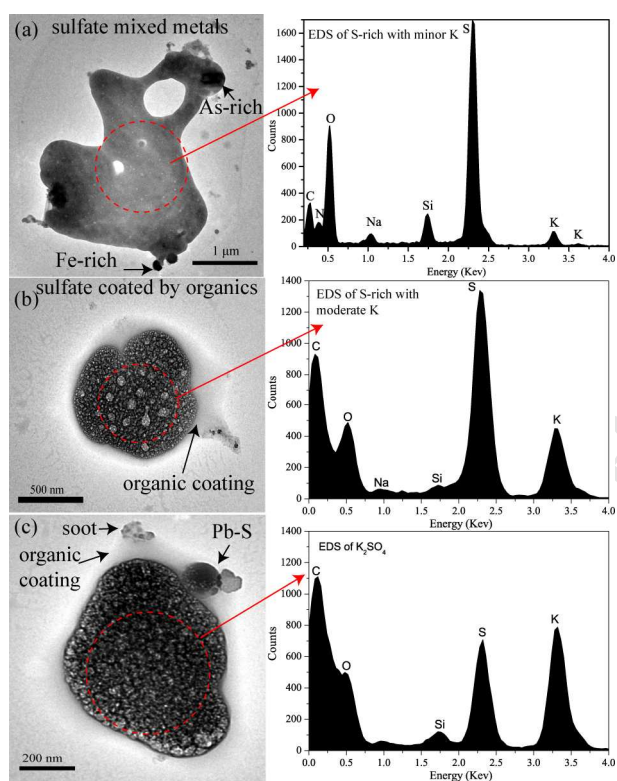


Figure 3 Three different types of individual S-rich particles. (a) S-rich particle with minor K mixed with one As-rich particle and one Fe-rich particle. EDS data obtained from INCA software under channel 5. (b) S-rich particle with moderate K coated by organics. (c) K_2SO_4 particle mixed with organic coating, soot, and Pb-S. EDS data obtained from INCA software under channel 4.

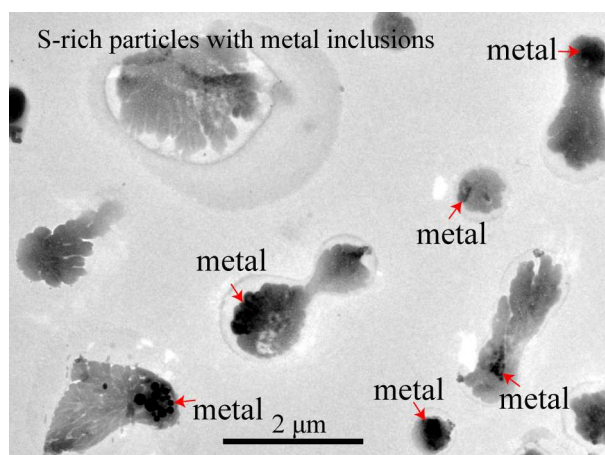


Figure 4 One low-magnification TEM image showing metal inclusions in S-rich

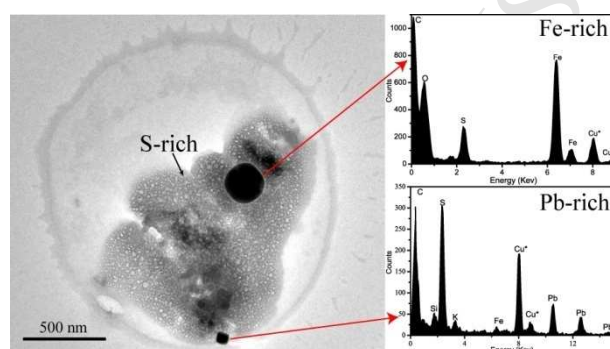


Figure 5 TEM image and EDS of two metal inclusions in one S-rich particle.

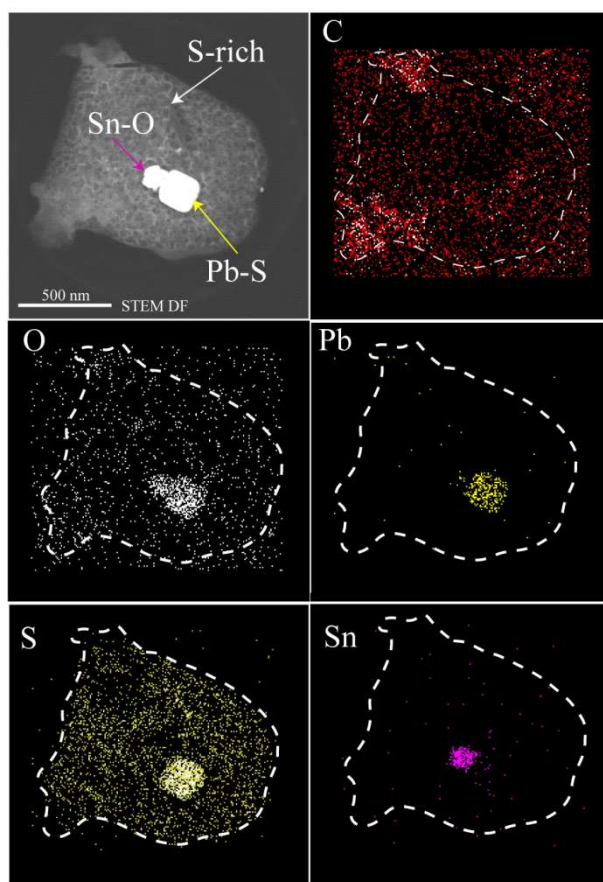


Figure 6 Elemental mapping of an individual metal-bearing particle obtained from the STEM. A dark-field TEM image of the individual particle and each elemental distribution are shown.

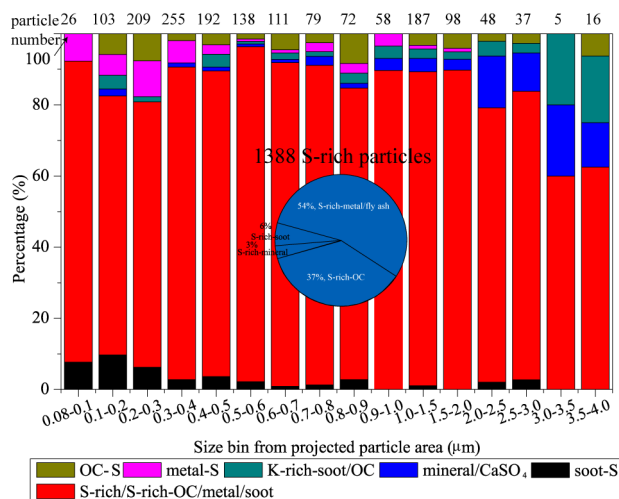


Figure 7 Proportions of aerosol particles collected at Mt. Lu during 11 August to 23 September, 2011 in acid precipitation area. A total of 1634 aerosol particles were identified by their different morphology and composition. The number of the analyzed aerosol particles in different size ranges is shown above each column.

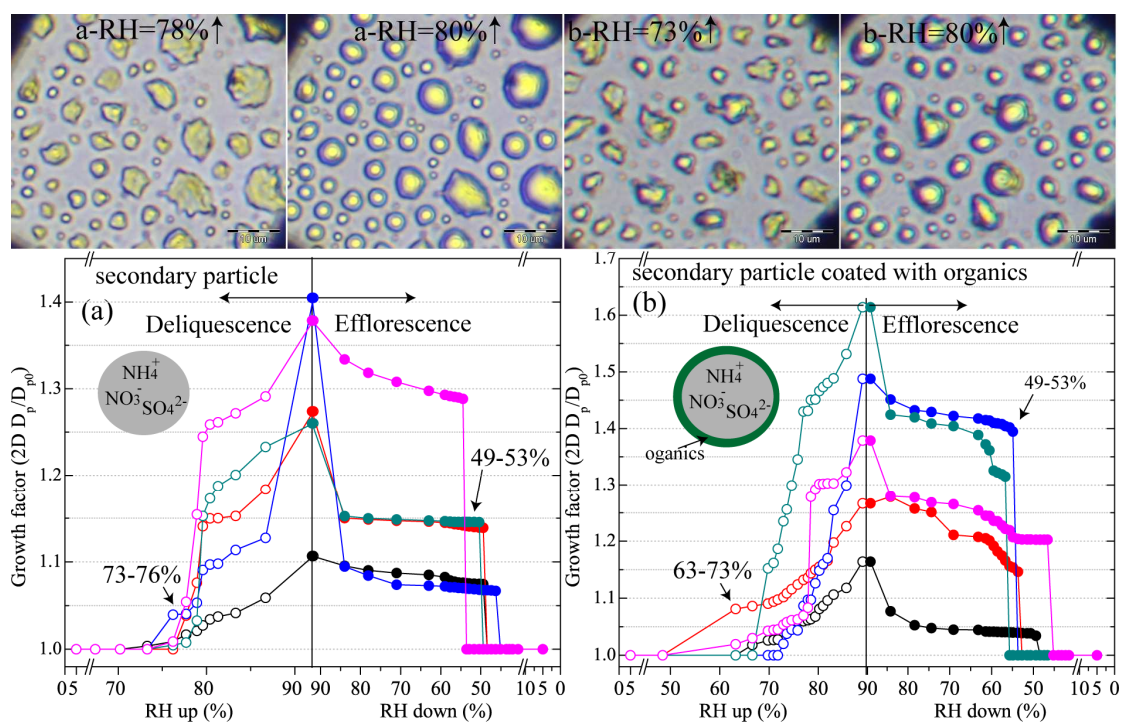


Figure 8 Deliquescence and efflorescence of each particle with one color from 3% to 90% RH. (a) the sample collected on 4 September, 2011 containing secondary particles (b) the sample collected on 5 September, 2011 containing secondary particles with organic coating. Compositions of individual particles in the two samples were examined by TEM/EDS as shown in Figure S6. Mixing state and composition of individual particles were described in the scheme.

Highlights:

- (1) SO_4^{2-} is the dominant ion in aerosol particles
- (2) Aerosol particles dominated by sulfate start to deliquesce at 63-76%
- (3) Large amounts of nano-sized metal particles embedded in 37% S-rich particles
- (4) SO_2 of long range transport from industries and fired-power plants in the YRD.

Composition and hygroscopicity of aerosol particles at Mt. Lu in

South China: Implications for acid precipitation

WeiJun Li^{1*}, Jianwei Chi¹, Zongbo Shi², Xinfeng Wang¹, Bin Chen¹, Yan Wang³, Tao Li³, Jianmin Chen^{1,3*}, Daizhou Zhang⁴, Zifa Wang⁵, Chune Shi⁶, Liangke Liu⁷, Wenxing Wang¹

¹Environment Research Institute, Shandong University, Jinan, Shandong 250100, China

²School of Geography, Earth and Environmental Sciences, University of Birmingham, UK

³School of Environment Science and Engineering, Shandong University, Jinan, Shandong 250100, China

⁴Faculty of Environmental and Symbiotic Sciences, Prefectural University of Kumamoto, Kumamoto 862-8502, Japan

⁵State Key of Laboratory of Atmospheric Boundary Physics and Atmospheric Chemistry, Institute of Atmospheric Physics, Chinese Academy of Sciences, Beijing 100029, China

⁶Anhui Institute of Meteorological Sciences, Anhui Institute of Meteorological Sciences, Hefei, 230031 China

⁷Nanjing University of information science and technology, Jiangsu, 210044 China

Corresponding Email: liweijun@sdu.edu.cn (W.J. Li) and jmchen@sdu.edu.cn (J.M. Chen)

Supporting information includes 8 Figures

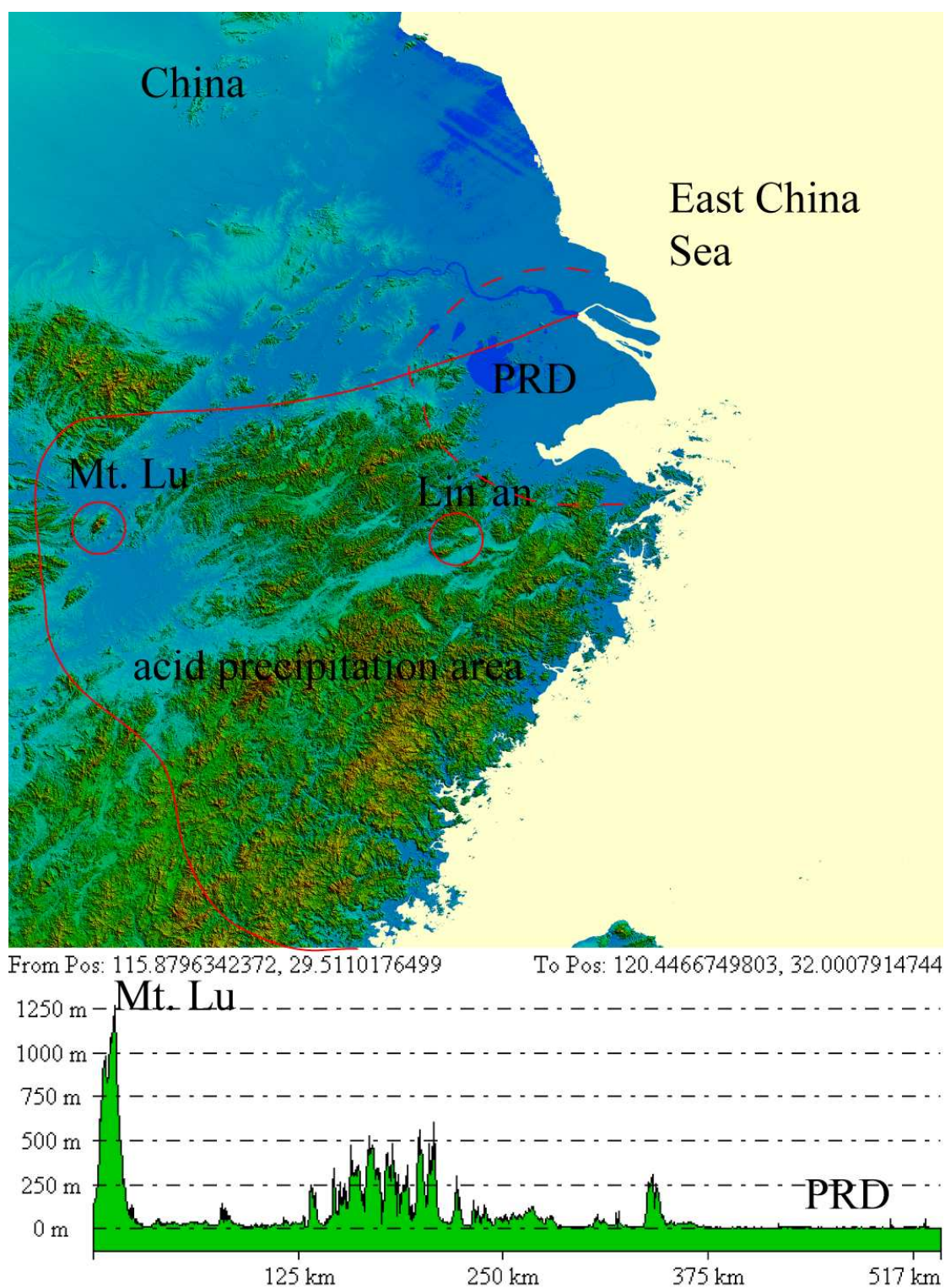


Figure S1 Terrain of South China and terrain profile of from PRD (East) to Mt. Lu (West). The map sourced from the website at <http://srtm.csi.cgiar.org/>

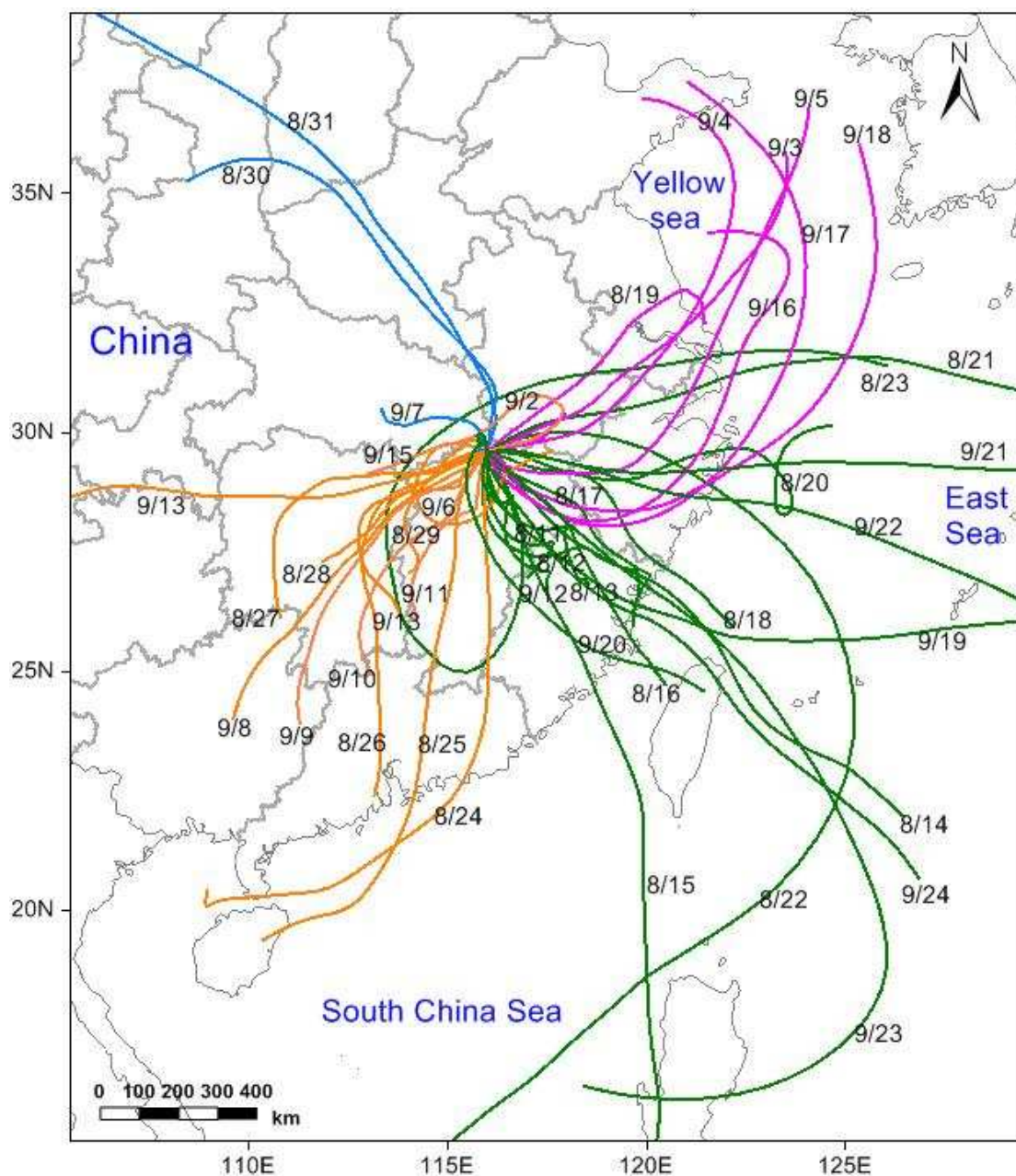


Figure S2 48-h Back trajectories of air masses arriving at 1500 m at Mt. Lu during 14 August -24 September, 2013. Most the trajectories were from South, East, and Northeast of Mt. Lu.

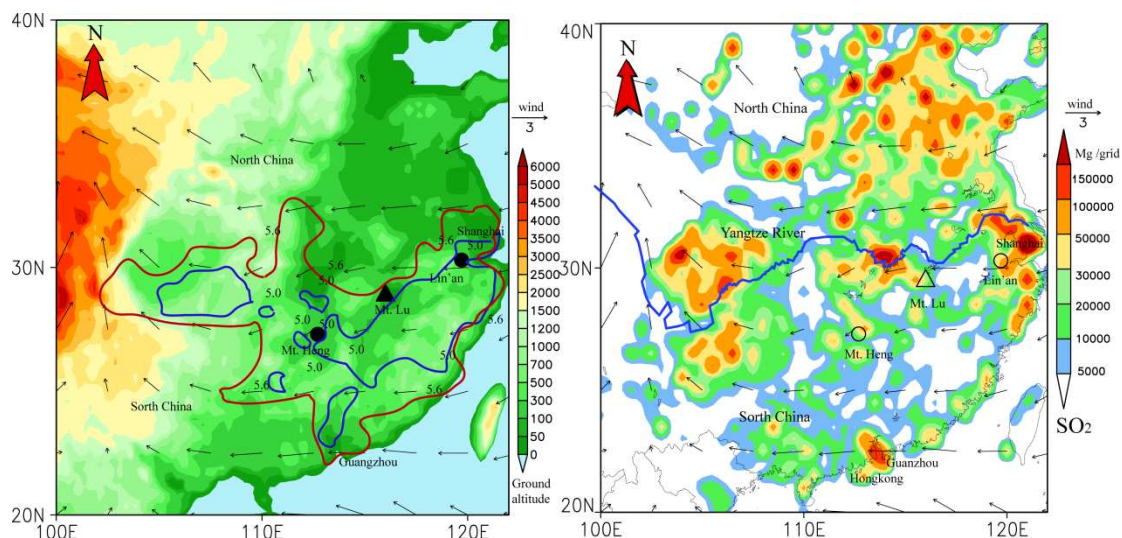


Figure S3 Topography and Asian summer monsoon. (a) Acid precipitation area over the highland area and summer wind during the sampling period (August and September of 2011 of meteorological model projection). The data of acid precipitation area were obtained from the Annual Environment Report of China in 2011 (b) SO₂ emission distributions and summer wind during the sampling period (SO₂ data from (Zhang et al., 2009)).

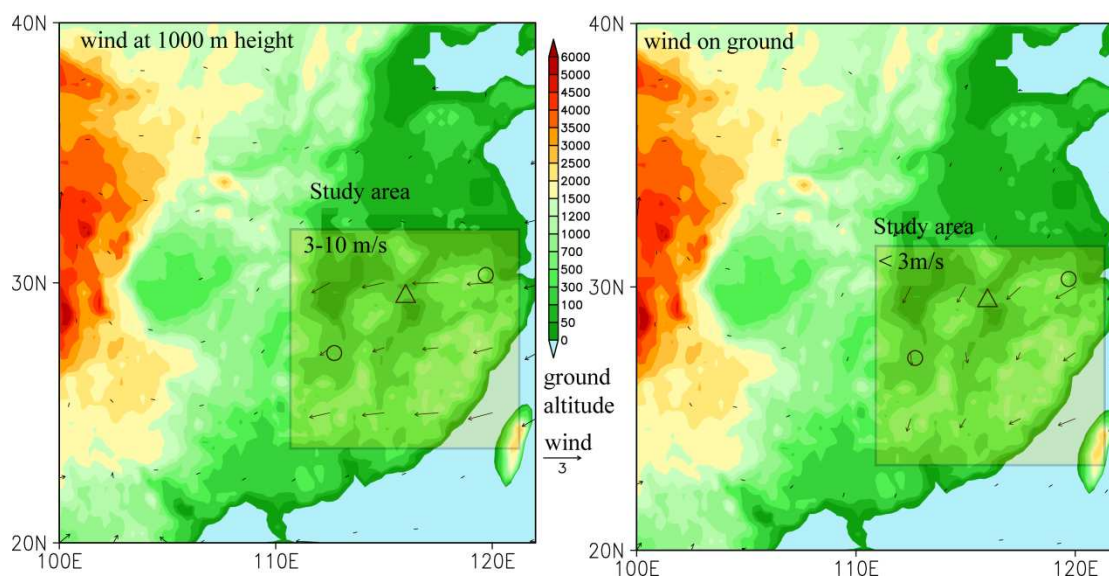


Figure S4 Wind direction and speed in different heights in August and September of 2011 in South China (a) wind at 1000 m height (b) wind on ground level. NCEP/NCAR global reanalysis data were used for projection of wind vector maps (Kalnay et al., 1996).

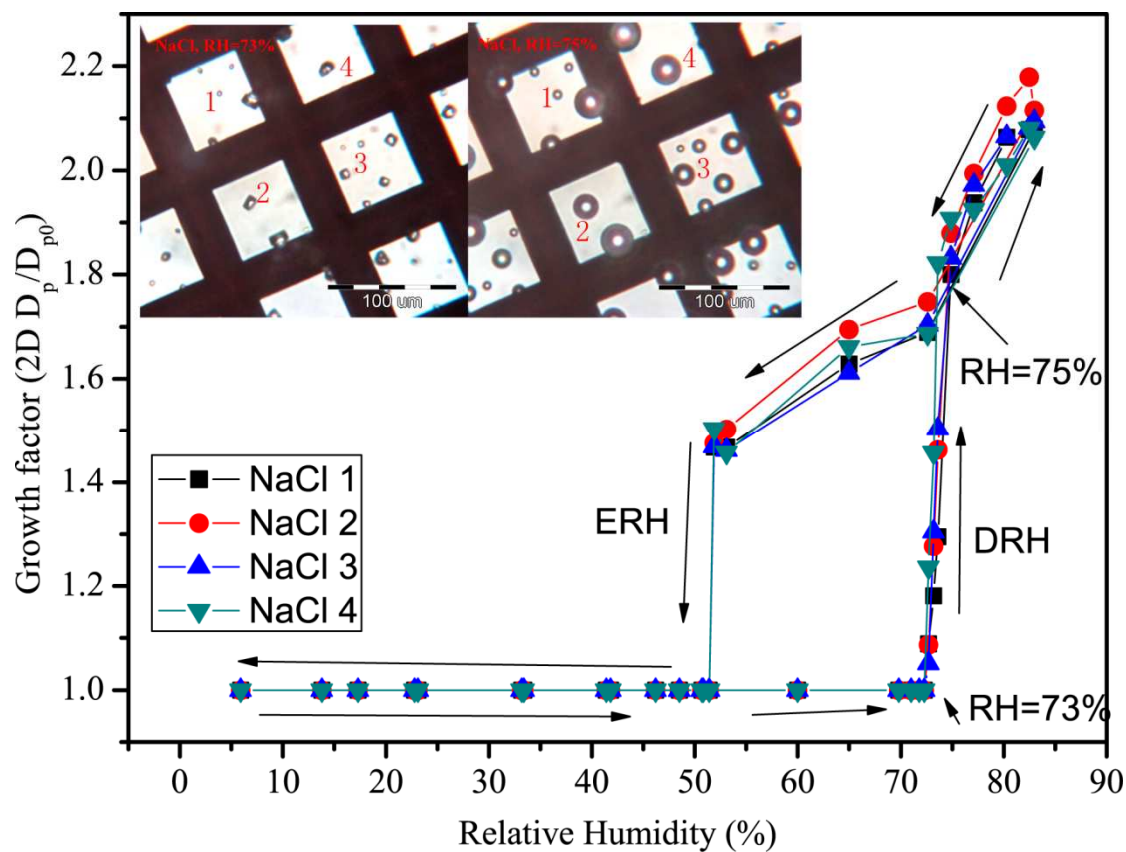


Figure S5 Humidifying and dehydration curves for the laboratory-generated NaCl particle collected on a TEM grid. Deliquescence relative humidity of pure NaCl is at 73-75%, which is consistent with the previous studies.

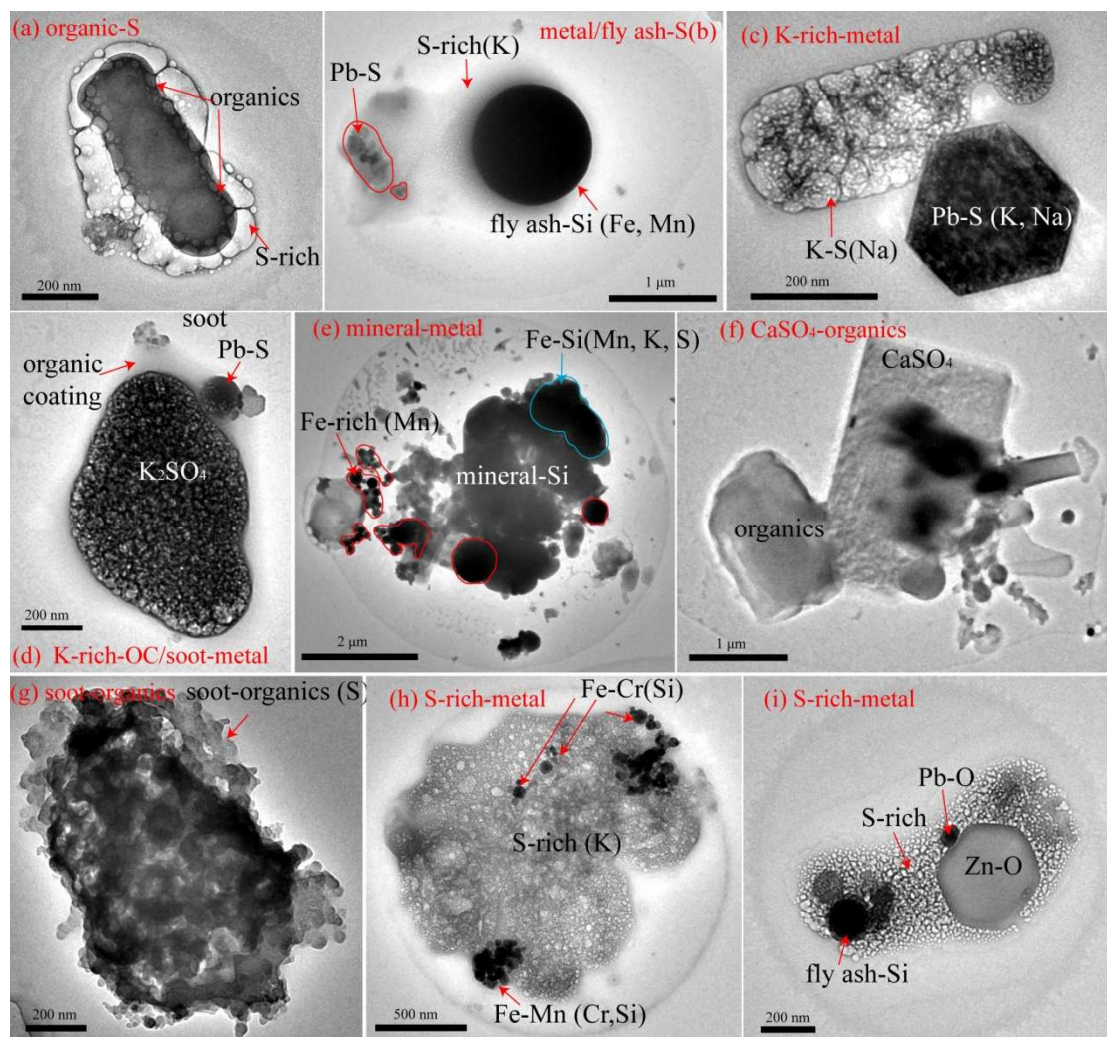


Figure S6 Different types of individual particles based on morphology and compositions

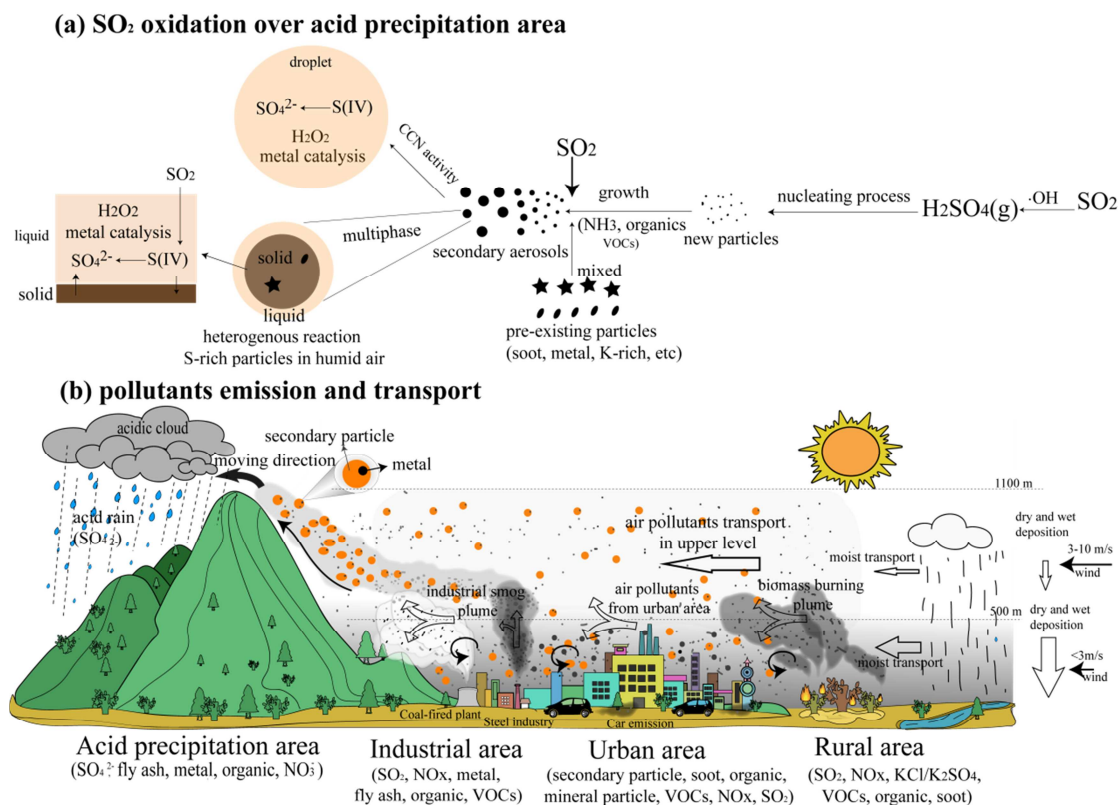


Figure S7 Conceptual model summarizing acid rain or cloud formation from anthropogenic pollutants. (a) SO₂ transformation over acid precipitation area. (b) pollutants emission and transportation. (1) air pollutants include the major gases and aerosols emitted from industrial area, urban area, and biomass burning in rural area. (2) air pollutants can be transported long distance into acid precipitation area in upper level and large amounts of secondary particles form in the air. (3) humid air and frequent rains limit vertical transport of urban pollutants from ground level into the upper atmosphere but not for smog plumes from tall stacks in industrial areas and biomass burning.

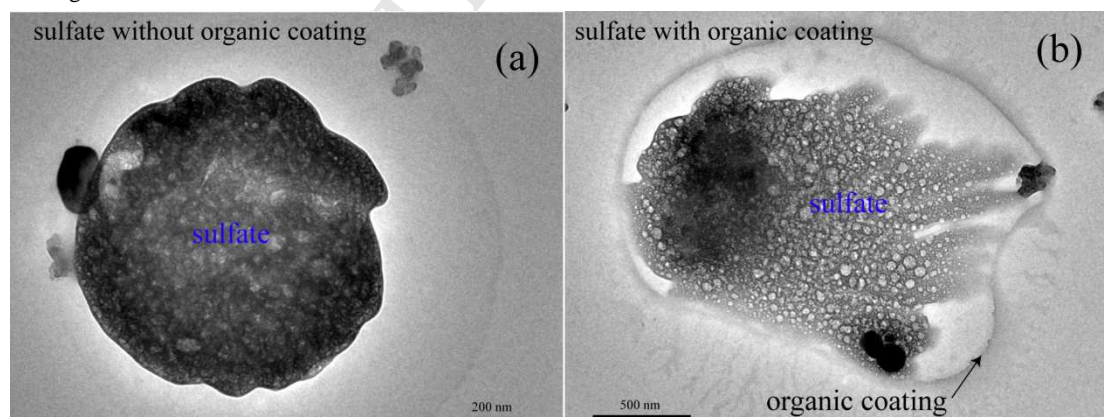


Figure S8 Sulfate particles without/with organic coating from the two different aerosol samples examined by TEM/EDS. After the TEM analysis, hygroscopic properties of aerosol particles in the two samples were studied in Figure 8.

References:

Kalnay, E., Kanamitsu, M., Kistler, R., Collins, W., Deaven, D., Gandin, L., Iredell, M., Saha, S., White, G., Woollen, J., Zhu, Y., Leetmaa, A., Reynolds, R., Chelliah, M., Ebisuzaki, W., Higgins, W.,

- Janowiak, J., Mo, K.C., Ropelewski, C., Wang, J., Jenne, R., Joseph, D., 1996. The NCEP/NCAR 40-Year Reanalysis Project. *Bulletin of the American Meteorological Society* 77 (3), 437-471.
- Zhang, Q., Streets, D.G., Carmichael, G.R., He, K.B., Huo, H., Kannari, A., Klimont, Z., Park, I.S., Reddy, S., Fu, J.S., Chen, D., Duan, L., Lei, Y., Wang, L.T., Yao, Z.L., 2009. Asian emissions in 2006 for the NASA INTEX-B mission. *Atmos. Chem. Phys.* 9 (14), 5131-5153.

ACCEPTED MANUSCRIPT